Frequency Offset and Symbol Timing Recovery in Flat-Fading Channels: A Cyclostationary Approach

Fulvio Gini, *Member, IEEE*, and Georgios B. Giannakis, *Fellow, IEEE*

***Abstract*— Two open-loop algorithms are developed for estimating jointly frequency offset and symbol timing of a linearly modulated waveform transmitted through a frequency-flat fading channel. The methods exploit the received signal's second-order cyclostationarity and, with respect to existing solutions: 1) they take into account the presence of time-selective fading effects; 2) they do not need training data; 3) they do not rely on the Gaussian assumption of the complex equivalent low-pass channel process; and 4) they are tolerant to additive stationary noise of any color or distribution. Performance analysis of the proposed methods using Monte Carlo simulations, unifications, and comparisons with existing approaches are also reported.**

***Index Terms*—Cyclostationarity, fading, synchronization.**

I. Introduction

DEMODULATION in digital communication systems requires knowledge of symbol timing and frequency offset. Mistiming and frequency drifts arise due to propagation, Doppler effects, and mismatch between transmit and receive oscillators. Both data-aided and nondata-aided feedforward (or open-loop) estimation structures have been proposed. Block (or batch) schemes include the feedforward data-aided frequency estimators proposed in [6], [9], and [11], which exploit the information signal's autocorrelation sequence to estimate the frequency offset. They do not account for fading and are simpler than the maximum likelihood, but are not bandwidth-efficient because they rely upon the training data of a preamble. The alternative is nondata-aided structures that recover synchronization parameters from the received data, exploiting only side information concerning the statistics of the information signal.

With fading effects, present in mobile cellular terrestrial radio systems [16], or in ionospheric channels [15], the synchronization problem is even more challenging. In [18] and [10], nondata-aided open-loop algorithms were proposed for joint frequency offset and symbol timing estimation in frequency-flat fading channels. The performance of [18] and [10] was simulated for both time- and frequency-selective fading environments, but the analytical results were derived assuming constant fading over the entire burst.

In this paper we propose an approach for fully digital nondata-aided joint frequency offset and symbol timing estimation of a linearly modulated waveform transmitted through a frequency-flat fading channel. Our approach exploits second-order cyclostationarity of the sampled received sequence and considers nonconstant fading over the entire burst. Moreover, the proposed algorithms can be used in a data-aided scenario without any change, if the appropriate preamble is employed.

A synchronization method relying explicitly on the cyclostationarity of the oversampled data was also proposed in [17], but fading effects were not considered. In continuous-time, [18] formed the instantaneous product of the received signal with its delayed-conjugated replica, and proved it periodic with period equal to the symbol interval. Although included in the original model, fading effects were argued to be small and were omitted from the instantaneous product prior to extracting its Fourier coefficients that were used for frequency offset and timing estimation [18]. Despite superficial resemblance, the approach herein relies on periodicity of discrete-time ensemble products of oversampled data, and fading effects are included in the cyclostationary (CS) statistics used to form consistent estimators of the synchronization parameters. The term CS processes and the role of cyclostationarity in communications dates back to Bennett [1]. Even if not clearly acknowledged, cyclostationarity has been exploited for synchronization purposes by many authors (see, e.g., [13], [10], and [5]). The underlying common idea is to use nonlinear combinations of the data to reveal periodic components containing synchronization parameters. In this paper, we attempt to unify and improve upon these approaches within a *discrete-time* CS framework.

The rest of the paper is organized as follows. In Section II we derive discrete-time models of the fading channel and the received signal, and introduce our modeling assumptions. The relationships between synchronization parameters, cyclic correlation, and cyclic spectrum of the observed sequence are derived in Sections III and IV, respectively. In Section V we show how to estimate the cyclic correlation and the cyclic spectrum consistently. The estimation algorithms and their performance can be found in Section VI along with unifications and comparisons with existing approaches. Finally, conclusions are drawn in Section VII.

Paper approved by E. Panayirci, the Editor for Synchronization and Equalization of the IEEE Communications Society. Manuscript received January 7, 1997; revised September 18, 1997. This work was supported by the National Science Foundation under Grant NSF-MIP 9 424 305. This paper was presented in part at the 1st IEEE Signal Processing Workshop on Wireless Communications, Paris, France, April 16–18, 1997.

F. Gini is with the Department of Information Engineering, University of Pisa, I-56126 Pisa, Italy (e-mail: gini@iet.unipi.it).

G. B. Giannakis is with the Department of Electrical Engineering, University of Virginia, Charlottesville, VA 22903-2442 USA (e-mail: georgios@virginia.edu).

Publisher Item Identifier S 0090-6778(98)02128-X.

II. Modeling and Problem Statement

The complex envelope of a linearly modulated signal, transmitted through a frequency-flat fading channel [8], [15, Ch. 14], [18], is received as

$$r_c(t) = \mu_c(t)e^{j(2\pi f_e t+\theta)}\sum_l w(l)g_c^{(\mathrm{tr})}(t-\epsilon T-lT)+n_c(t) \tag{1}$$

where $\mu_c(t)$ is the fading-induced multiplicative (or pattern) noise, $g_c^{(\mathrm{tr})}(t)$ is the transmitter's signaling pulse, T is the symbol period, $w(l)$'s are the complex information symbols, f_e is the frequency offset, θ is the initial phase, and ϵT is the propagation delay within a symbol period ($0 \le \epsilon < 1$). Complex additive noise $n_c(t)$ is assumed stationary but not necessarily white and/or Gaussian (subscript c denotes continuous-time signals).

After the receiving matched filter $g_c^{(\mathrm{rec})}(t)$, the signal $x_c(t) = r_c(t) * g_c^{(\mathrm{rec})}(t)$ ($*$ denotes convolution) is (over)sampled at a rate P/T, where P is an integer. We thus obtain the following discrete-time data:

$$x(n) = \mu(n)e^{j((2\pi/P)f_eTn+\theta)}\sum_l w(l)g(n-lP)+v(n) \tag{2}$$

with $x(n) := x_c(t)|_{t=nT/P}$, $\mu(n) := \mu_c(t)|_{t=nT/P}$, $v(n) := n_c(t) * g_c^{(\mathrm{rec})}(t)|_{t=nT/P}$, and $g(n) := g_c(t-\epsilon T)|_{t=nT/P}$, where $g_c(t)$ is the combined impulse response of the known transmitter and receiver filters in cascade $g_c(t) := g_c^{(\mathrm{tr})}(t) * g_c^{(\mathrm{rec})}(t)$. For the moment, we do not invoke any specific assumption on the shape of $g_c(t)$.

Models (1) and (2) are valid as long as:

1) the fading distortion $\mu_c(t)$ is approximately constant over a pulse duration or, equivalently, the Doppler spread $B_\mu T$ is small [15, Ch. 14], where B_μ denotes the bandwidth of $\mu_c(t)$. Typical values for practical systems range from $B_\mu T = 10^{-3}$ (very slow fading) to $B_\mu T = 10^{-1}$ (very fast fading) [12];
2) the frequency offset is small compared to the symbol rate, so that the mismatch of the receive-filter $g_c^{(\mathrm{rec})}(t)$ due to f_e can be neglected. In [11], $f_eT \le 0.2$ was typically assumed (see also [9], [10], and [18]).

The following assumptions are imposed on (2).

(AS1): $w(n)$ is a zero-mean independently identically distributed (i.i.d.) sequence with values drawn from a finite-alphabet complex constellation, with variance σ_w^2.

(AS2): $\mu(n)$ is stationary complex process with autocorrelation $m_{2\mu}(\tau) := E\{\mu(n)\mu^*(n+\tau)\}$; the Fourier transform (FT) of $m_{2\mu}(\tau)$ is called *Doppler spectrum* [15, Ch. 14].

(AS3): $v(n)$ is a wide-sense stationary complex process, independent of $\mu(n)$.

(AS4): $v(n)$ satisfies the so-called `mixing conditions` (see e.g., [3] and [4]), which state that the kth-order cumulant of $v(n)$ at lag $\boldsymbol{\tau} := (\tau_1, \tau_2, \cdots, \tau_{k-1})$, denoted by $c_{kv}(\boldsymbol{\tau})$, is absolutely summable: $\Sigma_{\boldsymbol{\tau}} |c_{kv}(\boldsymbol{\tau})| < \infty \forall\ k$. Similarly, we assume that $\mu(n)$ is mixing as well.

Mixing requires that sufficiently separated samples are approximately independent and is satisfied by all finite memory signals in practice. (AS4) will prove useful in establishing consistency of our estimation algorithms.

The goal here is to derive estimates of f_e and ϵ in (1) based on N consecutive samples $\{x(n); n = 0, 1, \cdots, N-1\}$ from (2), corresponding to $\lfloor N/P \rfloor$ transmitted symbols ($\lfloor a \rfloor$ denotes integer part of a). If $w(n)$ is given (data-aided scenario), and the distributions of $\mu(n)$ and $v(n)$ are known (e.g., $v(n)$ is Gaussian or i.i.d. non-Gaussian with known parameters), then maximum-likelihood (ML) estimation of f_e and ϵ is possible although computationally demanding. We seek consistent, albeit computationally efficient, estimates that cannot only initialize the nonlinear search required by ML estimates in the data-aided case, but, most importantly, remain operational in the blind (nondata-aided) scenario with realistic fading and colored noise processes of unknown distributions.

In the ensuing section we establish that the fractionally-sampled discrete-time process $x(n)$ is CS with period P, and show how this property leads to consistent estimators of f_e and ϵ.

III. Cyclic Correlation Approach

The time-varying correlation of a general nonstationary process $x(n)$ is defined as $m_{2x}(n;\tau) := E\{x(n)x^*(n+\tau)\}$, where τ is an integer lag. Signal $x(n)$ is termed second-order CS with period P iff there exists an integer P such that $m_{2x}(n;\tau) = m_{2x}(n+kP;\tau) \forall\ n, k$ (see, e.g., [7] and [3]). With $x(n)$ given by (2), and under assumptions (AS1)–(AS3), we have

$$m_{2x}(n;\tau) = \sigma_w^2 m_{2\mu}(\tau)e^{-j(2\pi/P)f_eT\tau}\sum_l g(n-lP)g^*\cdot(n+\tau-lP)+m_{2v}(\tau). \tag{3}$$

To establish that $x(n)$ in (2) is CS with period P, consider (3) and replace n with $n+kP$

$$\begin{aligned} m_{2x}(n+kP;\tau) &= \sigma_w^2 m_{2\mu}(\tau)e^{-j(2\pi/P)f_eT\tau} \\ &\quad\cdot\sum_l g(n+kP-lP)g^*(n+kP+\tau-lP)+m_{2v}(\tau) \\ &= \sigma_w^2 m_{2\mu}(\tau)e^{-j(2\pi/P)f_eT\tau} \\ &\quad\cdot\sum_i g(n-iP)g^*(n+\tau-iP)+m_{2v}(\tau) = m_{2x}(n;\tau) \end{aligned} \tag{4}$$

where in deriving the second equality we set $i = l-k$.

For a fixed τ, (4) shows that $m_{2x}(n;\tau)$ is periodic in n with period P. Thus, it has discrete Fourier series coefficients given by $\mathcal{M}_{2x}(k;\tau) := (1/P)\Sigma_{n=0}^{P-1} m_{2x}(n;\tau)\exp(-j(2\pi/P)kn)$, which are periodic with respect to (w.r.t.) k with period P; $\mathcal{M}_{2x}(k;\tau)$ is termed cyclic correlation and $\{2\pi k/P, k = -P/2, \cdots, P/2-1\}$ are called cyclic frequencies or cycles. From (3), the cyclic

correlation turns out to be[1]

$$\mathcal{M}_{2x}(k;\tau)=\frac{\sigma_w^2}{P}m_{2\mu}(\tau)e^{-j(2\pi/P)f_eT\tau}\cdot\sum_n g(n)g^*(n+\tau)e^{-j(2\pi/P)kn}+m_{2v}(\tau)\delta(k). \tag{5}$$

We wish to reveal the dependence of $\mathcal{M}_{2x}(k;\tau)$ on the time epoch ϵT which was absorbed in $g(n)$ when we passed from (1) to (2). Let us denote the FT of $g(n)$ as $G(f):=\Sigma_n\, g(n)\exp(-j2\pi fn)$ and use Parseval's relation to rewrite the sum in (5) as

$$\sum_n g(n)g^*(n+\tau)e^{-j(2\pi/P)kn}=\int_{-1/2}^{1/2}G^*\left(\beta-\frac{k}{P}\right)G(\beta)e^{-j2\pi\beta\tau}\,d\beta. \tag{6}$$

Now recall that $g(n):=g_c(t-\epsilon T)|_{t=nT/P}$ and suppose that the bandwidth B_g of $g_c(t)$ is less than $P/(2T)$; thus, sampling at a rate P/T does not introduce aliasing. In the absence of aliasing, we have (e.g., [14, Ch. 3])

$$G(f)=\frac{1}{T_s}G_c(F)e^{-j2\pi F\epsilon T}|_{F=(f/T_s)}=\frac{1}{T_s}G_c\left(\frac{f}{T_s}\right)e^{-j2\pi f\epsilon P},\qquad \text{for } |f|\le 1/2 \tag{7}$$

where $G_c(F):=\int_{-\infty}^{\infty}g_c(t)e^{-j2\pi Ft}\,dt, F:=f/T_s$ denotes the continuous-time frequency variable and $T_s=T/P$ is the sampling period. Inserting (7) in (6) and then (6) in (5), we obtain

$$\mathcal{M}_{2x}(k;\tau)=\frac{\sigma_w^2}{P}m_{2\mu}(\tau)e^{-j(2\pi/P)f_eT\tau}\cdot e^{-j2\pi k\epsilon}G_2(k;\tau)+m_{2v}(\tau)\delta(k) \tag{8}$$

where we defined $G_2(k;\tau):=(P/T)\int_{-P/(2T)}^{P/(2T)}G_c^*(\beta-k/T)G_c(\beta)e^{-j2\pi\beta\tau T/P}\,d\beta$.

We observe from (8) that frequency offset and symbol timing appear as separable one-dimensional complex exponentials in the two-dimensional sequence $\mathcal{M}_{2x}(k;\tau)$: f_e w.r.t. the lag τ and ϵ w.r.t. the cycle k. We will use this observation to estimate f_e and ϵ separately.

Note now that $G_2(k;\tau)$ in (8) is known because the signaling pulse $g_c(t)$ is known. Hence, we can "compensate" for it by multiplying (8) with $G_2^{-1}(k;\tau)$, provided that $(k;\tau)\in\mathcal{I}_{G2}$, where $\mathcal{I}_{G2}:=\{(k;\tau)|G_2(k;\tau)\neq 0\}$. Upon defining $\mathcal{M}_2(k;\tau):=G_2^{-1}(k;\tau)\mathcal{M}_{2x}(k;\tau)$ we can rewrite (8) as

$$\mathcal{M}_2(k;\tau)=\frac{\sigma_w^2}{P}m_{2\mu}(\tau)e^{-j(2\pi/P)f_eT\tau}e^{-j2\pi k\epsilon}+G_2^{-1}(k;\tau)m_{2v}(\tau)\delta(k). \tag{9}$$

Noise $v(n)$ affects the cyclic correlation in (9) at cycle $k=0$. To avoid it, we henceforth consider $k\neq 0$. Moreover, (9) suggests cancelling ϵ by multiplying $\mathcal{M}_2$ terms with cycle frequencies k and $-k$.

[1]To derive (5) we used the identity $\Sigma_{p=0}^{P-1}\,\Sigma_{l=-\infty}^{+\infty}\,f(p-lP)=\Sigma_{n=-\infty}^{+\infty}\,f(n)$, with $f(n):=g(n)g^*(n+\tau)\exp(-j(2\pi/P)kn)$.

Thus, denoting with arg the unwrapped phase, we can retrieve f_e from the phase of a "compensated" (or "normalized") cyclic correlation product as follows:

$$f_e=-\frac{P}{4\pi T\tau}\arg\{\mathcal{M}_2(k;\tau)\mathcal{M}_2(-k;\tau)\},\quad \text{for } k>0;\tau\in[1,L_\tau] \tag{10}$$

where L_τ denotes the maximum τ in $\mathcal{I}_{G2}$.

Given the frequency offset f_e, the time epoch ϵ can be theoretically derived as [c.f. (9)]

$$\epsilon=-\frac{1}{2\pi k}\arg\{\mathcal{M}_2(k;\tau)e^{j(2\pi/P)f_eT\tau}\},\quad \text{for } k\neq 0;\tau\in[0,L_\tau]. \tag{11}$$

Relationships (10) and (11) form the basis for the estimation algorithms developed in this paper. Estimating f_e and ϵ based on (10) and (11) may require phase unwrapping. In the next section we will avoid phase unwrapping by working in the cyclic spectrum domain (see also [13] for a thorough discussion on phase unwrapping issues).

Remark 1: Having retrieved f_e and ϵ, we can obtain the correlation of the fading from (9) as $m_{2\mu}(\tau)=(\sigma_w^2/P)\mathcal{M}_2(k;\tau)\exp\{-j2\pi(k\epsilon+\tau f_eT/P)\}$ for $k\neq 0$ and $\tau\in\mathcal{I}_{G2}$. Based on $m_{2\mu}(\tau)$, parametric (e.g., autoregressive) models can be fit to $\mu(n)$. Such models may be potentially useful for parsimonious characterization, classification, or tracking of possible variations in the fading process (see also [19]).

IV. Cyclic Spectrum Approach

By definition, the cyclic spectrum of $x(n)$ is the FT of $\mathcal{M}_{2x}(k;\tau)$ w.r.t. τ [7], [3], i.e., $\mathcal{S}_{2x}(k;f):=FT_{\tau\to f}[\mathcal{M}_{2x}(k;\tau)]=\Sigma_\tau\mathcal{M}_{2x}(k;\tau)\,\exp(-j2\pi f\tau)$. From (9), we obtain

$$\mathcal{S}_2(k;f):=\mathcal{G}_2^{(-1)}(k;f)*\mathcal{S}_{2x}(k;f)=\mathcal{S}_{2\mu}\left(f+\frac{f_eT}{P}\right)e^{-j2\pi k\epsilon}+\mathcal{G}_2^{(-1)}(k;f)*\mathcal{S}_{2v}(f)\delta(k) \tag{12}$$

where $\mathcal{G}_2^{(-1)}(k;f):=FT_{\tau\to f}[G_2^{-1}(k;\tau)]$ and $\mathcal{S}_{2\mu}(f):=FT_{\tau\to f}[m_{2\mu}(\tau)]$. It is now customary to introduce a further assumption on the fading channel characteristics.

(AS5): $\mu(n)$ is a complex low-pass process with power spectral density $\mathcal{S}_{2\mu}(f)$ peaking at a known frequency; w.l.o.g. we assume that $\mathcal{S}_{2\mu}(f)$ peaks at $f=0$ (see [15, Ch. 14] and also [2], [12], and [20]).

Under (AS5), f_e can be recovered by peak-picking the magnitude of (12) as

$$f_e=-\frac{P}{T}\,\arg\,\max_f|\mathcal{S}_2(k;f)|,\qquad k\neq 0 \tag{13}$$

and the time epoch can be found from the phase at the peak

$$\epsilon=-\frac{1}{2\pi k}\,\arg\left\{\mathcal{S}_2\left(k;-\frac{f_eT}{P}\right)\right\},\qquad k\neq 0. \tag{14}$$

It is worth observing that ambiguity due to spectral folding does not occur in (13) if $|f_eT|<P/2$, while the estimator in (10) requires $|f_eT|<P/4$ with $\tau=1$.

In addition, note that (AS5) is not strictly necessary; for example, the Doppler spectrum could also have two peaks as long as they are known, but in this case the structure of the frequency estimator (13) should be modified accordingly. In Section VI, we will make use of (10) and (11) or (13) and (14) to derive consistent estimators of f_e and ϵ. But first, we need sample estimates of $\mathcal{M}_{2x}(k;\tau)$ and $\mathcal{S}_{2x}(k;f)$.

V. Cyclic Statistics

Since we do not have access to ensemble cyclic quantities, we should estimate them from finite samples. We estimate $\mathcal{M}_{2x}(k;\tau)$ from a single record $\{x(n)\}_{n=0}^{N-1}$, using the (normalized) fast Fourier transform (FFT) of the product $x(n)x^*(n+\tau)$ as follows:

$$\hat{\mathcal{M}}_{2x}(k;\tau):=\frac{1}{N}\sum_{n=0}^{N-\tau-1}x(n)x^*(n+\tau)e^{-j(2\pi/P)kn},\qquad \tau>0. \tag{15}$$

Negative lags are obtained by symmetry $\mathcal{M}_{2x}(k;-\tau)=\exp(j2\pi k\tau/P)\mathcal{M}_{2x}^*(k;\tau)$. Under (AS4), $\hat{\mathcal{M}}_{2x}$ is asymptotically unbiased and mean square sense (m.s.s.) consistent; i.e., $\lim_{N\to\infty}\hat{\mathcal{M}}_{2x}(k;\tau)\overset{\text{m.s.s.}}{=}\mathcal{M}_{2x}(k;\tau)$ [4]. As a consequence, the estimators of f_e and ϵ, obtained by replacing $\mathcal{M}_{2x}$ by $\hat{\mathcal{M}}_{2x}$ in (10) and (11), are asymptotically unbiased and consistent.

Similar reasoning applies to (13) and (14) when sample cyclic spectra are used in practice. Consistent estimates of the cyclic spectra can be obtained by windowing $\hat{\mathcal{M}}_{2x}(k;\tau)$ with $W^{(2L_g+1)}(\tau)$ having support $[-L_g,L_g],L_g\le L_\tau$, and Fourier transforming to obtain [3]

$$\hat{\mathcal{S}}_{2x}(k;f)=\sum_{\tau=-L_g}^{L_g}W^{(2L_g+1)}(\tau)\hat{\mathcal{M}}_{2x}(k;\tau)e^{-j2\pi f\tau}. \tag{16}$$

Alternatively, it has been shown in [3] that $\mathcal{S}_{2x}(k;f)$ can be estimated directly from the data, relying upon the so-called cyclic periodogram defined as

$$I_{2x}^{(N)}(k;f):=\frac{1}{N}X_N\left(\frac{k}{P}-f\right)X_N^*(-f),\qquad X_N(f):=\sum_{n=0}^{N-1}x(n)e^{-j2\pi fn}. \tag{17}$$

Note that $I_{2x}^{(N)}(0;f)$ denotes the conventional periodogram for stationary processes. Although the cyclic periodogram is an unbiased estimator of the cyclic spectrum, it is inconsistent. Under (AS4) it has been proven that smoothing $I_{2x}^{(N)}(k;f)$ with an appropriate spectral window $W^{(N)}(f)$, the cyclic spectral estimate

$$\hat{\mathcal{S}}_{2x}(k;f):=\frac{1}{N}\sum_{i=0}^{N-1}I_{2x}^{(N)}\left(k;\frac{i}{N}\right)W^{(N)}\left(f-\frac{i}{N}\right) \tag{18}$$

is consistent and asymptotically normal with computable variance [3]. As with stationary processes, windowing controls the bias-variance tradeoff encountered with cyclic spectral estimates. Without it, the variance of $\hat{\mathcal{S}}_{2x}(k;f)$ in (16) and (18) would not decrease as $N\to\infty$ (see [3] for rigorous statements and guidelines on the choice of windows).

It is worth noting at this point that if the record length N is small, then the estimates $\hat{\mathcal{M}}_{2x}(k;\tau)$ or $I_{2x}^{(N)}(k;f)$ should be zero-padded to sufficiently large length N_{zp} prior to the FFT so that the frequency bins $\{f_i=i/N_{zp}\}_{i=0}^{N_{zp}-1}$ in (27) are small enough to allow accurate estimation of f_e. In [11], it is reported that the Cramer–Rao lower bound (CRLB) for frequency estimation of a pure sinusoid in additive white Gaussian noise (AWGN) is given by $\mathrm{CRLB}(f_eT)=(3\mathrm{SNR}^{-1})/(2\pi^2N(N^2-1))$. Therefore, for the FFT bin sizes to be compatible with this limit, N_{zp} must be large enough to satisfy $1/N_{zp}<\sqrt{\mathrm{CRLB}(f_eT)}$. Alternatively, high-resolution algorithms (such as MUSIC, Kumaresan–Tufts, or matrix pencil) can be used, but these directions are beyond the scope of this work.

VI. Estimators and Comparisons

The effects of pattern and additive noise on our estimation algorithms can be potentially reduced by averaging (10) and (11) over $(k;\tau)\in\mathcal{I}_g/\{k=0,-P/2\}$ to obtain

$$\hat{f}_e=-\frac{P}{4\pi T(P/2-1)L_g}\sum_{k=1}^{P/2-1}\sum_{\tau=1}^{L_g}\cdot\frac{1}{\tau}\arg\{\hat{\mathcal{M}}_2(k;\tau)\hat{\mathcal{M}}_2(-k;\tau)\} \tag{19}$$

$$\hat{\epsilon}=-\frac{1}{2\pi(P-1)(L_g+1)}\sum_{\substack{k=-P/2\\k\neq0}}^{P/2-1}\sum_{\tau=0}^{L_g}\cdot\frac{1}{k}\arg\{\hat{\mathcal{M}}_2(k;\tau)e^{j(2\pi/P)f_eT\tau}\}. \tag{20}$$

Correspondingly, the cyclic-spectrum-based estimators are derived from (13) and (14) as

$$\hat{f}_e=-\frac{P}{T(P-1)}\sum_{\substack{k=-P/2\\k\neq0}}^{P/2-1}\arg\max_f|\hat{\mathcal{S}}_2(k;f)| \tag{21}$$

$$\hat{\epsilon}=-\frac{1}{2\pi(P-1)}\sum_{\substack{k=-P/2\\k\neq0}}^{P/2-1}\frac{1}{k}\arg\left\{\hat{\mathcal{S}}_2\left(k;-\frac{\hat{f}_eT}{P}\right)\right\}. \tag{22}$$

A remark is now in order on complexity issues.

Remark 2: From (19) to (22) we observe that complexity increases with P, but there is also a tradeoff in selecting P even from an estimation viewpoint. Although more samples are collected as P increases, their correlation increases too, which is known to increase the estimators' variance. Hence, as in [2], moderate values of P are recommended $(P=4,8,16)$ and the corresponding moderate increase in complexity is justified by the improvement evidenced in our simulations (see Fig. 3). Note that if one wishes to average only a subset of all possible cycles, complexity may be reduced by replacing the FFT in (15) with the chirp-FFT [14, p. 623]. In addition, performance improves at the expense of increased complexity

as the number of lags L_g increases. But, as with P, there is a tradeoff also with L_g—one should not average over lags that are far away from the origin (say $|\tau|>16$) because the accuracy of the corresponding sample cyclic correlations decreases due to reduced averaging [c.f. (15)].

Expressions (19)–(22) are valid for arbitrary pulse shapes. Next, we will specialize $g_c(t)$ to the commonly used raised cosine pulse[2] (see, e.g., [11] and [18]). Such a choice will not only reduce complexity but also will allow us to assess performance and compare our estimators with existing methods.

(AS6): $g_c(t)$ is a raised cosine pulse, truncated and delayed by t_0 to assure causality $g_c(t)=g_{rc}(t-t_0)u(t)\cong g_{rc}(t-t_0)$, where $u(t)$ is the unit step function and $g_{rc}(t)$ is the noncausal (even w.r.t. t) raised cosine pulse [15, Ch. 9]. Let $B_g=(1+\alpha)/2T$ denote its bandwidth, where α is the so-called rolloff factor $(0\le\alpha\le 1)$.

In the following, we will show that when $g_c(t)$ is a raised cosine, we can easily "compensate" for the presence of G_2 without normalizing $\hat{\mathcal{M}}_{2x}$ and $\hat{\mathcal{S}}_{2x}$ to obtain $\hat{\mathcal{M}}_2$ and $\hat{\mathcal{S}}_2$.

A. Estimators with Raised Cosine Pulse

Under (AS6) and denoting by $G_{rc}(F)$ the FT of $g_{rc}(t)$, we have that $G_2(k;\tau)$ in (8) can be written as

$$G_2(k;\tau)=\frac{P}{T}e^{j(\pi k/P)\tau}e^{-j2\pi(t_0/T)k}\int_{-P/(2T)}^{P/(2T)}G_{rc}\cdot\left(\beta-\frac{k}{2T}\right)G_{rc}\left(\beta+\frac{k}{2T}\right)e^{-j2\pi\beta\tau T/P}\,d\beta. \quad (23)$$

Thanks to the particular shape of $G_{rc}(F)$, the integral is real and even w.r.t. τ [15, p. 546]. Recall also that $G_{rc}(f/T_s)=0$ for $|f|>(1+\alpha)/(2P)$, and since $0\le\alpha\le 1$, we have $G_{rc}(f/T_s)=0$ for $f\notin[-1/P,1/P]$; hence, the product $G_{rc}((f-k/2P)/T_s)G_{rc}((f+k/2P)/T_s)$ in (23) will be nonzero only for $k=0,\pm1$. As a result, $G_2(k;\tau)$ in (23) and $\mathcal{M}_{2x}(k;\tau)$ in (8) will be nonzero only for the cycles $k=0$, $k=1$, and $k=-1$.

To obviate the additive noise, we will thus rely only on $\hat{\mathcal{M}}_{2x}(1;\tau)$ and $\hat{\mathcal{M}}_{2x}(-1;\tau)$ to estimate f_e and ϵ as follows [c.f. (19) and (20)]:

$$\hat{f}_e=-\frac{P}{4\pi TL_g}\sum_{\tau=1}^{L_g}\frac{1}{\tau}\ \arg\{\hat{\mathcal{M}}_{2x}(1;\tau)\hat{\mathcal{M}}_{2x}(-1;\tau)\} \quad (24)$$

$$\hat{\epsilon}=-\frac{1}{4\pi(L_g+1)}\sum_{\tau=0}^{L_g}\cdot[\arg\{\hat{\mathcal{M}}_{2x}(1;\tau)e^{j(2\pi/P)(\hat{f}_eT-(1/2))\tau}e^{j(2\pi t_0/T)}\}-\arg\{\hat{\mathcal{M}}_{2x}(-1;\tau)e^{j(2\pi/P)(\hat{f}_eT+(1/2))\tau}e^{-j(2\pi t_0/T)}\}] \quad (25)$$

where t_0 denotes the known delay of $g_{rc}(t)$.

As concerning the estimators based on the cyclic spectrum, they can be derived observing that in this case $\mathcal{G}_2(k;f):=FT_{\tau\to f}[G_2(k;\tau)]=G_{rc}(f/T_s)G_{rc}(f/T_s-k/T)\exp(-j2\pi kt_0/T)$, where $F=f/T_s$ and $T_s=T/P$. Recalling that $G_2(k;\tau)\neq 0$ in (23) for $k=0,\pm1$, and excluding $k=0$ to suppress noise, we find the cyclic spectrum as

$$\mathcal{S}_{2x}(k;f)=\mathcal{S}_{2\mu}\left(f+\frac{f_eT}{P}\right)*[G_{rc}\left(\frac{fP}{T}\right)G_{rc}\cdot\left(\frac{fP}{T}-\frac{k}{T}\right)]e^{-j2\pi((t_0/T)+\epsilon)k},\qquad k=\pm1. \quad (26)$$

Plugging in the square bracketed term of (26) the raised cosine spectrum [15, p. 547], it turns out (by setting derivatives equal to zero) that the maxima occur at $f=1/(2P)$ for $k=1$, and $f=-1/(2P)$ for $k=-1$. These maxima are shifted by f_eT/P due to the convolution by $\mathcal{S}_{2\mu}$ in (26); hence, $\arg\max_f|\hat{\mathcal{S}}_{2x}(1;f)|=-(\hat{f}_eT-1/2)/P$ and $\arg\max_f|\hat{\mathcal{S}}_{2x}(-1;f)|=-(\hat{f}_eT+1/2)/P$, from which we obtain easily

$$\hat{f}_e=-\frac{P}{2T}[\arg\max_f|\hat{\mathcal{S}}_{2x}(1;f)|+\arg\max_f|\hat{\mathcal{S}}_{2x}(-1;f)|]). \quad (27)$$

Similarly, subtracting the phase at $\hat{f}_e$, we estimate the time epoch as

$$\hat{\epsilon}=-\frac{1}{4\pi}\left[\arg\left\{\hat{\mathcal{S}}_{2x}\left(1;-\frac{\hat{f}_eT}{P}\right)e^{j2\pi(t_0/T)}\right\}-\arg\left\{\hat{\mathcal{S}}_{2x}\left(-1;-\frac{\hat{f}_eT}{P}\right)e^{-j2\pi(t_0/T)}\right\}\right]. \quad (28)$$

Expressions (24)–(25) and (27)–(28) are the main results of this paper specialized for raised cosine pulses. Their performance will be compared next with existing algorithms. Summarizing, under (AS1)–(AS6) the estimators (24)–(25) and (27)–(28) are asymptotically unbiased and m.s.s. consistent, independent of the color and distribution of the additive noise and the fading distortion.

B. Comparison with Scott–Olasz (S–O)

For comparison purposes we have derived the discrete-time version of the estimators proposed by Scott and Olasz (S–O) in [18]. With the notation adopted so far, they are expressed as

$$\hat{f}_e=-\frac{1}{4\pi T}\ \arg\{\hat{\mathcal{M}}_{2x}(1;P)\hat{\mathcal{M}}_{2x}(-1;P)\} \quad (29)$$

$$\hat{\epsilon}=-\frac{1}{2\pi}\ \arg\{\hat{\mathcal{M}}_{2x}(1;\tau)e^{j(2\pi/P)(\hat{f}_eT-(1/2))\tau}e^{j(2\pi t_0/T)}\}. \quad (30)$$

The $\hat{\epsilon}$ estimator originally proposed in [18] contained the term $\exp(j(2\pi/P)\hat{f}_eT\tau)$ in order to compensate for the contribution of the frequency offset. However, the terms $\exp(-j\pi\tau/P)$ and $\exp(j2\pi t_0/T)$ that are necessary to compensate for the effects of $g_c(t)$ were not included (see [18, eq. (2.18)]).

Computer simulations were run to verify the efficacy of the proposed algorithms in frequency-flat fading channel environments. The linear modulation format was 4-quadrature

[2]This means that both $g_c^{(\mathrm{tr})}(t)$ and $g_c^{(\mathrm{rec})}(t)$ are square-root raised cosine pulses.

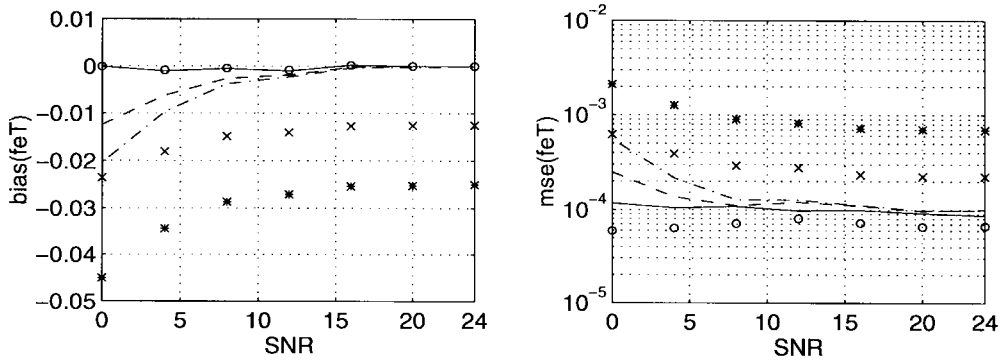

(a) (b)

Fig. 1. (a) Bias and (b) MSE of $\hat{f}_eT$ versus SNR (dB). Estimator (24): $f_eT = 0.0$ (solid line), $f_eT = 0.1$ (dashed line), and $f_eT = 0.2$ (dash–dot line). S–O: $f_eT = 0.0$ (circles), $f_eT = 0.1$ ($\times$-marks), and $f_eT = 0.2$ (stars).

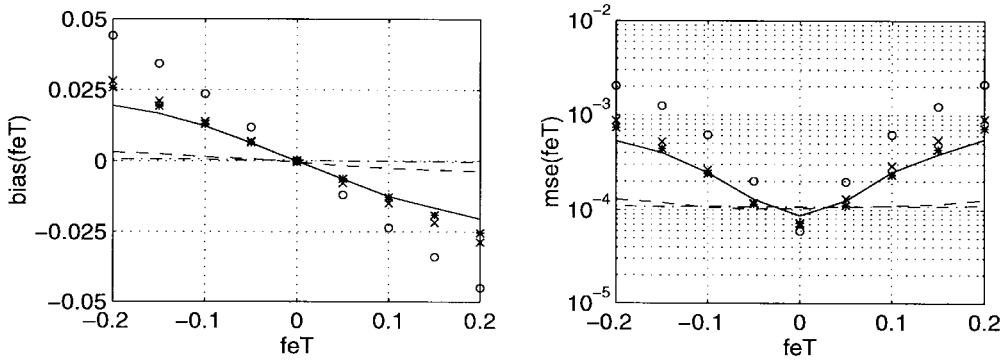

(a) (b)

Fig. 2. (a) Bias and (b) MSE of $\hat{f}_eT$ versus f_eT. Estimator (24): $\mathrm{SNR} = 0$ dB (solid line), $\mathrm{SNR} = 8$ dB (dashed line), $\mathrm{SNR} = 16$ dB (dash–dot line). S–O: $\mathrm{SNR} = 0$ dB (circles), $\mathrm{SNR} = 8$ dB ($\times$-marks), $\mathrm{SNR} = 16$ dB (stars).

amplitude modulation (QAM) and $w(l)$ i.i.d. symbols were generated with $\sigma_w^2 = 2$. The transmit and receive filters were the square-root raised cosine pulses with 50% rolloff ($\alpha = 0.5$) and the receive filter was simulated as a finite-impulse response (FIR) filter with $(7P+1)$ taps; thus, $t_0 = 7T/2$ and the equivalent time duration of the FIR impulse response was $2t_0 + T/P$. The additive noise $v(n)$ was generated by passing zero-mean complex Gaussian deviates through the square-root raised cosine filter to yield autocorrelation sequence $m_{2v}(\tau) = \sigma_v^2 g_{rc}(\tau)$. The land–mobile channel is generally modeled by the Clarke's model [16]. However, as pointed out in [2], it is difficult to efficiently simulate the exact mobile channel spectrum with conventional filters. So, we followed the usual practice of using a low-pass filter with sharp 3-dB cutoff. In [2], an FIR filter with 256 taps was adopted, while [20] used a Butterworth filter with three poles to simulate the fading distortion. In our simulations, $\mu(n)$ was modeled as a low-pass autoregressive process of order $Q = 5$, with real multiple poles at ρ. It can be shown that the 3-dB bandwidth of such a filter (i.e., the so-called Doppler spread that in Section II we denoted by $B_\mu T$) is related to the multiple pole ρ through the equation $(\sqrt[Q]{2}-1)\rho^2 - 2[\sqrt[Q]{2} - \cos(2\pi B_\mu T)]\rho + \sqrt[Q]{2} - 1 = 0$.

Note that our algorithms put no constraint on the distribution of the fading distortion. Under (AS1)–(AS5), consistency of the proposed $\hat{f}_e$ and $\hat{\epsilon}$ estimators is guaranteed irrespective of the distribution of $\mu(n)$. Only for simulation purposes, we assumed a Rayleigh channel, with $\mu(n)$ zero-mean complex circular Gaussian (w.l.o.g. we assumed also that $\sigma_\mu^2 = m_{2\mu}(0) = 1$). The signal-to-noise ratio (SNR) was defined as $\mathrm{SNR} := \sigma_w^2/\sigma_v^2$.

1) Frequency Offset Estimation—(24) Versus (29): An estimation interval of $L = 512$ symbols was assumed. Estimates of the cyclic correlation were obtained as in (15), with $P = 8$ samples per symbol interval, for a total of $N = 512 \times 8$ samples. The other parameters were chosen as $B_\mu T = 0.05$ (fast fading), $L_g = 16$, and $\epsilon = 0.375$. The results reported in Figs. 1 and 2 were obtained by averaging over 400 Monte Carlo trials. Fig. 1(a) shows the bias and Fig. 1(b) shows the mean square error (MSE) of the frequency offset estimator $\hat{f}_e$ (normalized to the symbol rate) versus SNR for different values of f_eT. Fig. 2(a) shows the bias and Fig. 2(b) shows the MSE of $\hat{f}_eT$ versus f_eT at three different SNR's. Except for $f_e = 0$, the proposed estimator in (24) outperforms the one in (29), especially at lower SNR's and greater frequency drifts. From the same set of simulations we derived the plots in Fig. 3 that depict MSE of $\hat{f}_eT$ versus SNR, for $\epsilon = 0.375$, $f_eT = 0.1$, and [Fig. 3(a)] different values of L_g or [Fig. 3(b)] different values of the oversampling factor P. Note that the S–O estimator (stars) does not depend on L_g, so only one plot for S–O is reported in Fig. 3(b). Larger L_g implies more averaging in (25) but also more noise in estimating $\hat{\mathcal{M}}_{2x}(k;\tau)$, which justifies the tradeoff observed in Fig. 3(a).

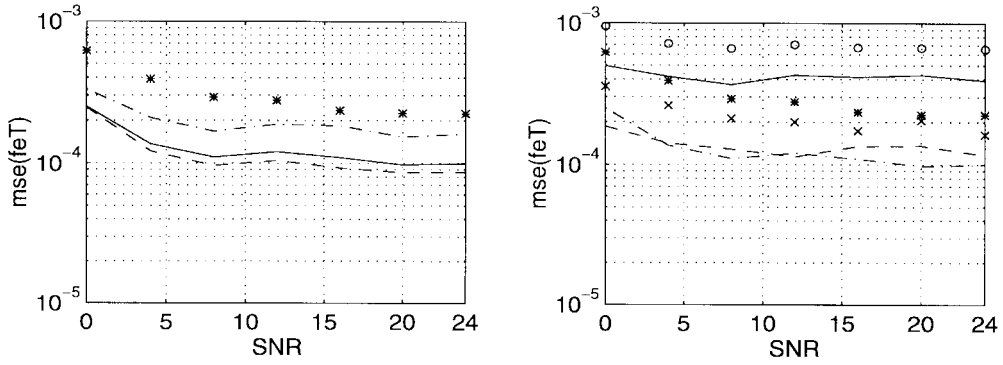

(a) (b)

Fig. 3. (a) MSE of $\hat{f}_eT$ versus SNR (dB). Estimator (24): $L_g = 8$ (solid line), $L_g = 16$ (dashed line), $L_g = 24$ (dash–dot line). S–O: stars. (b) MSE of $\hat{f}_eT$ versus SNR (dB). Estimator (25): $P = 4$ (solid line), $P = 8$ (dashed line), $P = 12$ (dash–dot line). S–O: $P = 4$ (circles), $P = 8$ ($\times$-marks), $P = 12$ (stars).

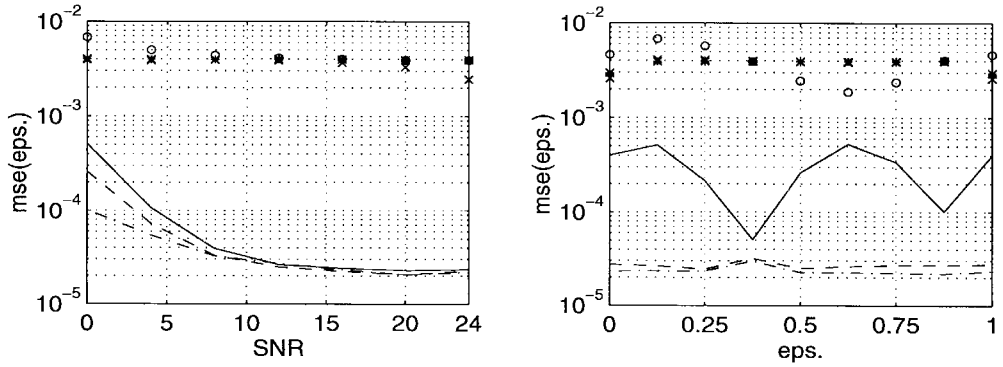

Fig. 4. (a) MSE of $\hat{\epsilon}$ versus SNR (dB) for different values of ϵ. Estimator (25): $\epsilon = 0.125$ (solid line), $\epsilon = 0.5$ (dashed line), $\epsilon = 0.875$ (dash–dot line). S–O: $\epsilon = 0.125$ (stars), $\epsilon = 0.5$ (circles), and $\epsilon = 0.875$ ($\times$-marks). (b) MSE of $\hat{\epsilon}$ versus ϵ at $\mathrm{SNR} = 8$ and 16 dB. Estimator (25): $\mathrm{SNR} = 0$ dB (solid line), $\mathrm{SNR} = 12$ dB (dashed line), $\mathrm{SNR} = 12$ dB (dash–dot line). S–O: $\mathrm{SNR} = 0$ dB (circles), $\mathrm{SNR} = 12$ dB ($\times$-marks), and $\mathrm{SNR} = 24$ dB (stars).

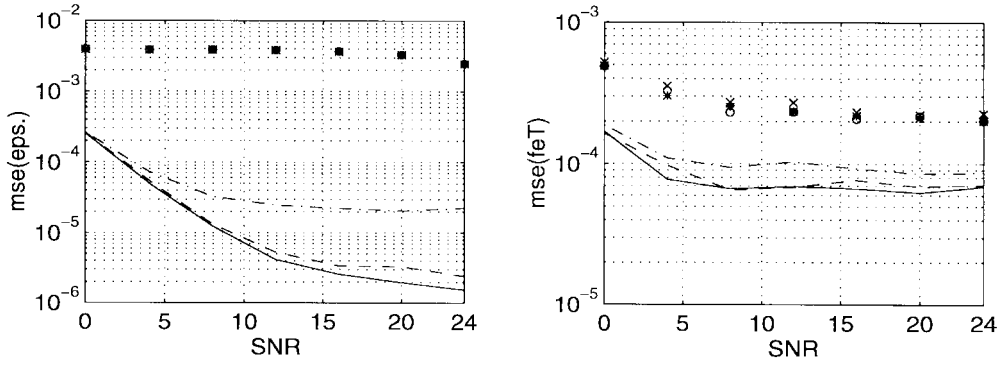

(a) (b)

Fig. 5. MSE of (a) $\hat{\epsilon}$ and (b) $\hat{f}_eT$ versus SNR (dB) for different values of the Doppler spread, $f_eT = 0.1, \epsilon = 0.5$. Estimators (24) and (25): $B_\mu T = 0.001$ (solid line), $B_\mu T = 0.01$ (dashed line), $B_\mu T = 0.05$ (dash–dot line). S–O: $B_\mu T = 0.001$ (stars), $B_\mu T = 0.01$ (circles), $B_\mu T = 0.05$ ($\times$-marks).

The improvement with increasing P observed in Fig. 3(b) is also expected since the effective data length increases as P increases. Nevertheless, the improvement is negligible for higher sampling rates and $P = 8$ seems to be a good tradeoff between performance gain and implementation complexity.

2) Time Epoch Estimation—(25) versus (30): Fig. 4(a) shows the MSE of $\hat{\epsilon}$ versus SNR for different values of ϵ, and Fig. 4(b) depicts the MSE of $\hat{\epsilon}$ versus ϵ for different values of SNR. The other parameters of the simulation were $f_eT = 0.1$, $B_\mu T = 0.05$, and $L_g = 16$. In Fig. 5(a) we plot the MSE of $\hat{\epsilon}$ and in Fig. 5(b) the MSE of $\hat{f}_eT$, versus SNR for $\epsilon = 0.5$, $f_eT = 0.1$, and different Doppler spread values $B_\mu T = 0.001$ (very slow fading), $B_\mu T = 0.01$ (slow fading), and $B_\mu T = 0.05$ (fast fading). Especially the performance of the timing estimator is considerably improved and justifies the extra computations involved in the proposed estimator relative to S–O.

3) Time Epoch Estimation—(28) versus (30): Fig. 6 shows the results of comparing the time epoch estimators (28) and (30), assuming an estimation interval of $L = 512$ symbols and

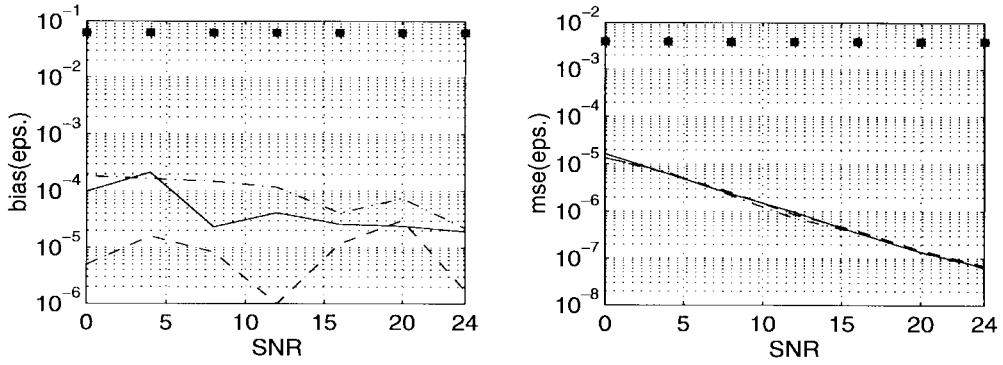

(a) (b)

Fig. 6. (a) Bias and (b) MSE of $\hat{\epsilon}$ versus SNR (dB) for different values of the frequency offset. Estimator (28): $f_eT = 0.0$ (solid line), $f_eT = 0.1$ (dashed line), $f_eT = 0.2$ (dash–dot line). S–O: $f_eT = 0.0$ (circles), $f_eT = 0.1$ ($\times$-marks), $f_eT = 0.2$ (stars).

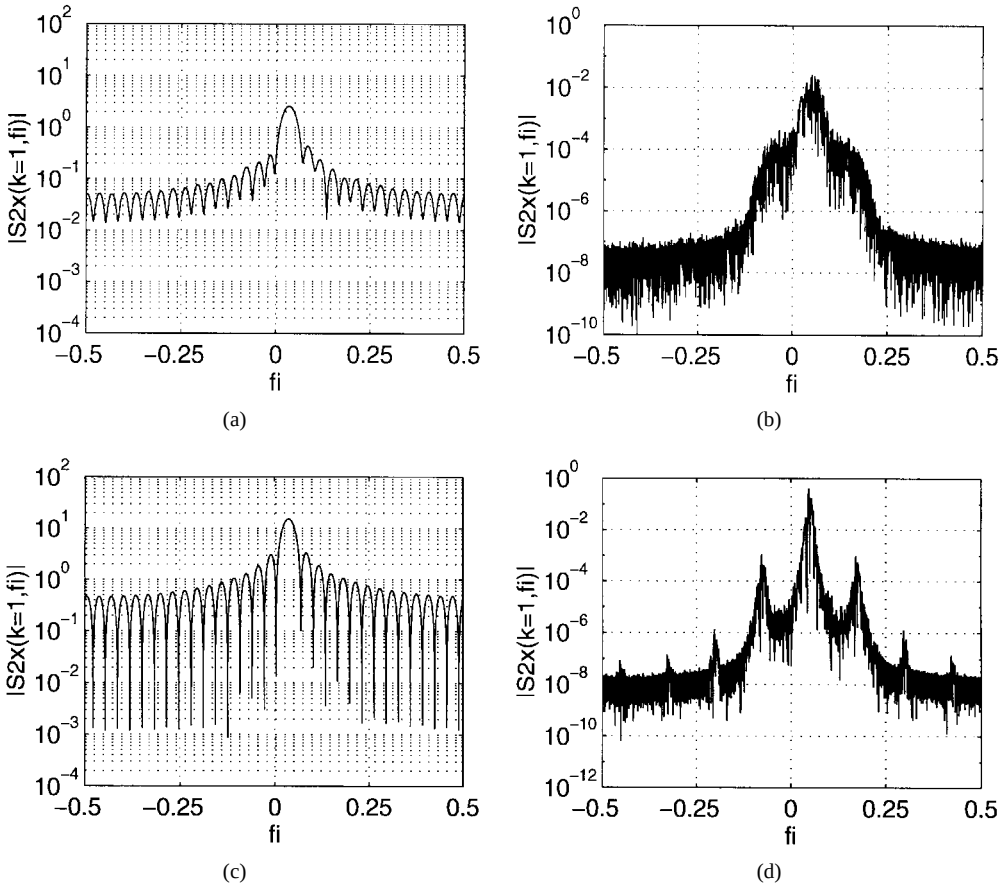

(a) (b) (c) (d)

Fig. 7. Cyclic spectrum $\hat{\mathcal{S}}_{2x}(1;f)$ estimated from (16) with (a) unknown 4-QAM and (c) known preamble, and from (18) with (b) unknown 4-QAM and (d) known preamble.

averaging over 400 Monte Carlo trials. The other parameters of the simulation were $P = 8$, $f_eT = 0.1$, $\epsilon = 0.875$, $L_g = 16$, and $B_\mu T = 0.05$. About an order of magnitude improvement is observed in both frequency offset and timing estimation with the proposed estimator which is FFT-based and thus computationally efficient as well.

Fig. 7(a) and (c) shows $\hat{\mathcal{S}}_{2x}(1;f)$ estimated via (16), while Fig. 7(b) and (d) depicts estimates computed as in (18). For Fig. 7(a) and (b) a 4-QAM modulation was used (nondata-aided case), while Fig. 7(c) and (d) refer to the case where a particular training sequence is used. It is evident that the random modulation reduces the resolution in $\hat{\mathcal{S}}_{2x}$. For both estimates in (16) and (18), a Kaiser window with parameter $\beta = 5$ [14, Ch. 7] was used. The other parameters of the simulation were $B_\mu T = 0.05$, $L = 128$, $P = 8$, SNR $= 0$ dB, $N_{zp} = 2^{17}$, $f_eT = 0.2$, $\epsilon = 0.875$, $L_g = 16$. Note also that, as predicted by (27), $\hat{\mathcal{S}}_{2x}(1;f)$ peaks (approximately) at $f = -(f_eT - 1/2)/P = 0.0375$.

To the best of the authors' knowledge, [18] and [10] are the only works dealing with nondata-aided open-loop algorithms for joint frequency offset and time epoch estimation in flat-fading channels. In [18], the effect of $\mu(n)$ on the estimators

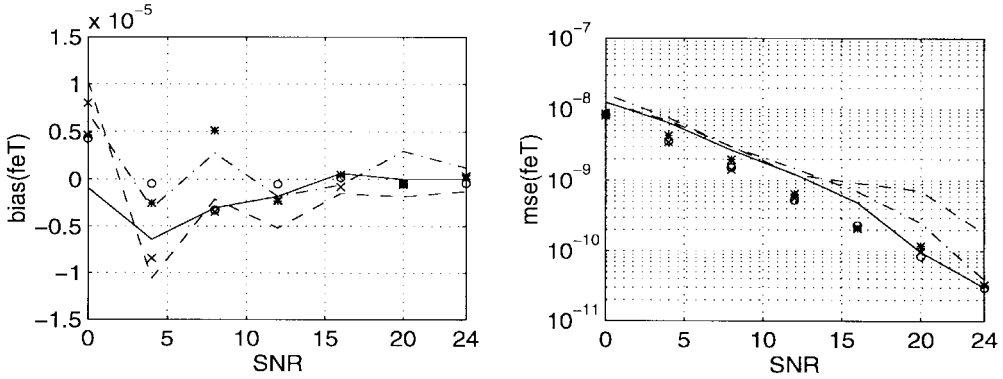

(a) (b)

Fig. 8. (a) Bias (a) and (b) MSE of $\hat{f}_e T$ versus SNR (dB) without fading ($B_\mu T = 0.0$). Estimator (27) with known preamble: $f_e T = 0.0$ (solid line), $f_e T = 0.1$ (dashed line), and $f_e T = 0.2$ (dash–dot line). M–M with known preamble: $f_e T = 0.0$ (circles), $f_e T = 0.1$ ($\times$-marks), and $f_e T = 0.2$ (stars).

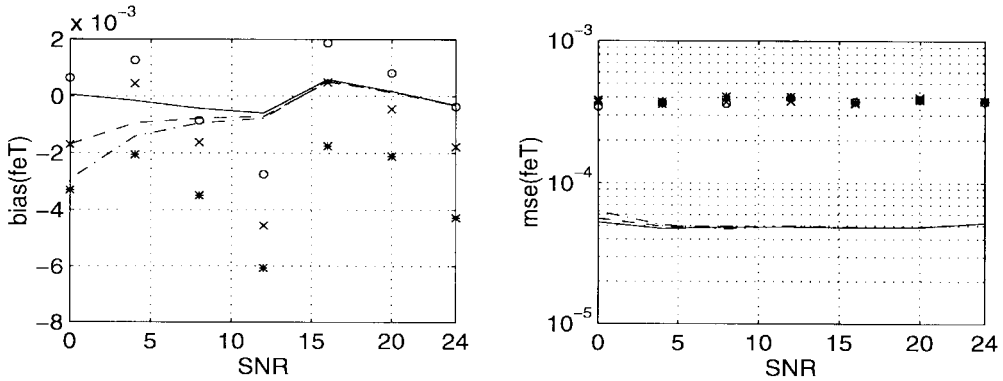

(a) (b)

Fig. 9. (a) Bias and (b) MSE of $\hat{f}_e T$ versus SNR (dB) in the presence of fading ($B_\mu T = 0.05$). Estimator (27) with known preamble: $f_e T = 0.0$ (solid line), $f_e T = 0.1$ (dashed line), and $f_e T = 0.2$ (dash–dot line). M–M with known preamble: $f_e T = 0.0$ (circles), $f_e T = 0.1$ ($\times$-marks), and $f_e T = 0.2$ (stars).

is not evident (in their analytical derivation the authors ignore fading). In [10], the fading distortion was considered constant over the entire burst (i.e., $\mu(n) = \mu$ for $n = 0, 1, \cdots, N-1$), so that $\mathcal{S}_{2\mu}(f) = \sigma_\mu^2 \delta(f)$, where $\delta(f)$ denotes the Dirac delta (note that in this case (AS5) is satisfied trivially).

Many works exist on data-aided open-loop frequency error estimation in AWGN (see, e.g., [9] and [11] and references therein), but fading effects are not included. In the next subsection, we will compare the estimator (27) with the one proposed in [11] [Mengali–Morelli (M–M)], in order to quantify the performance loss in (27) with respect to an algorithm tailored to a specific data-aided situation. On the other hand, we explore how performance improves by using (27) instead of the M–M estimator when time-selective fading is present.

C. Comparison with M–M

With the notation adopted so far, the M–M estimator can be expressed as [11]

$$\hat{f}_e = \frac{1}{2\pi T} \sum_{\tau=1}^{L/2} W^{(L/2)}(\tau)\ \arg\{\hat{r}_z(\tau)\hat{r}_z^*(\tau-1)\}$$
$$W^{(L/2)}(\tau) := \frac{12(L-\tau)(L-\tau+1) - 3L^2}{2L(L^2-1)} \tag{31}$$

where $\hat{r}_z(\tau) := (L-\tau)^{-1} \sum_{n=0}^{L-1} z(n)z^*(n+\tau)$ is the unbiased sample autocorrelation sequence of the data $z(n)$ collected by sampling at the symbol rate, and $W^{(L/2)}(\tau)$ is a window of length $L/2$. The estimator (31) assumes a preamble of known data and accurate timing information. To satisfy these assumptions, we chose as zero-mean preamble $\{w(l) = (1+j)(-1)^l, l = 0, 1, \cdots, L-1\}$, as required by (AS1). This preamble could come from a 4-phase-shift keying (PSK) constellation (as in [11]) or from a 4-QAM constellation.

Figs. 8 and 9 compare (27) with (31) under the assumption of perfect timing (even if (27) does not require timing recovery), known preamble, no fading effects, and AWGN $n_c(t)$. For the plots in Fig. 8 we averaged over 200 Monte Carlo trials with $L = 128, N_{zp} = 2^{17}, \alpha = 0.5, \epsilon = 0.5, P = 8$. As expected, the performance of the M–M algorithm is slightly better, although with training symbols the performance of (27) is close to that of M–M. Furthermore, there is no need to change the structure of the estimator in (27) so long as the preamble is zero mean. M–M performs better because it corresponds to an approximate ML approach under the above assumptions. In [11] it is also shown that the M–M algorithm is efficient, so the corresponding MSE shown in Fig. 8(b) coincides with the CRLB for AWGN channel. However, simulations show that the performance of

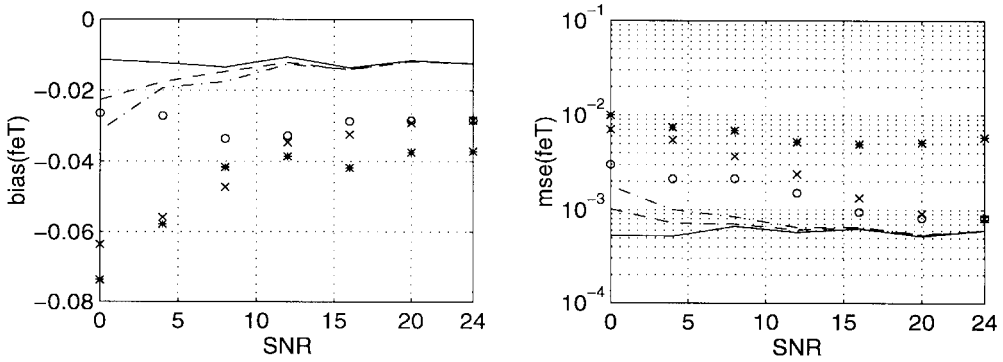

(a) (b)

Fig. 10. (a) Bias and (b) MSE of $\hat{f}_e T$ versus SNR (dB) in the presence of fading ($B_\mu T = 0.05$). Estimator (24): $f_e T = 0.0$ (solid line), $f_e T = 0.1$ (dashed line), and $f_e T = 0.2$ (dash–dot line). Estimator (27): $f_e T = 0.0$ (circles), $f_e T = 0.1$ ($\times$-marks), and $f_e T = 0.2$ (stars).

(31) degrades more rapidly than that of (27) or (24). This is illustrated in Fig. 9, under perfect timing recovery, known preamble and AWGN, but in the presence of fading distortion with Doppler spread $B_\mu T = 0.05$. The M–M algorithm does not guarantee consistent estimates in this case, while our algorithm does and, from this point of view, (27) and (24) may have more general use. Moreover, they do not employ training data, but require more samples relative to those required by data-aided algorithms (typically in the order of 100 symbols [11]).

It is interesting now to explore the relationship between estimators (31) and (24), which at first glance is not evident. Recall that the sequence $z(n)$ is stationary and is related to the oversampled CS sequence $x(n)$ in (2) via[3] $z(n) = x(nP)$; hence,

$$\hat{r}_z(\tau) = \frac{L}{L-\tau} \times \frac{1}{L} \sum_{n=0}^{L-1} z(n) z^*(n+\tau)$$
$$= \frac{L}{L-\tau} \times \frac{1}{L} \sum_{n=0}^{L-1} x(nP) x^*(nP+\tau P).$$

Let us now derive the expression of the zero-cycle ($k = 0$) cyclic moment that corresponds to the time-invariant (stationary) component of $x(n)$. From (15), we have $\hat{\mathcal{M}}_{2x}(0;\tau) = (1/LP) \sum_{n=0}^{LP-1} x(n) x^*(n+\tau)$, where L is the number of symbols. Thus, we can write

$$\hat{\mathcal{M}}_{2x}(0;\tau P) = \frac{1}{LP} \sum_{n=0}^{LP-1} x(n) x^*(n+\tau P)$$
$$= \frac{1}{P} \sum_{i=0}^{P-1} \hat{\mathcal{M}}_{2x}^{(i)}(0;\tau P)$$

where we defined $\hat{\mathcal{M}}_{2x}^{(i)}(0;\tau P) := (1/L) \sum_{n=0}^{L-1} x(i + nP) x^*(i + nP + \tau P)$; $\hat{\mathcal{M}}_{2x}^{(i)}(0;\tau P)$ can be thought of as the correlation of the ith stationary component $x_i(n) := x(nP + i)$ of the CS $x(n)$. It is thus evident that $\hat{r}_z(\tau) = (L/(L-\tau)) \hat{\mathcal{M}}_{2x}^{(0)}(0;\tau P)$ and hence

$$\hat{f}_e = \frac{1}{2\pi T} \sum_{\tau=1}^{L/2} W^{(L/2)}(\tau) \arg\cdot\{\hat{\mathcal{M}}_{2x}^{(0)}(0;\tau P) \hat{\mathcal{M}}_{2x}^{(0)}(0;\tau P - P)\}. \tag{32}$$

Note that we could use the estimator (32) with $\hat{\mathcal{M}}_{2x}(0;\tau P)$ instead of $\hat{\mathcal{M}}_{2x}^{(0)}(0;\tau P)$ in order to reduce additive and pattern noise. The price to be paid is in terms of complexity, since $\hat{\mathcal{M}}_{2x}(0;\tau P)$ requires oversampling by a factor P. The link between (24) and (31) is now evident if we recall (5), where frequency offset is present in the form of a complex harmonic w.r.t. the lag τ. From (32), we see that the M–M algorithm exploits the fact that frequency offset generates a phase shift $2\pi f_e T$ among adjacent values of the correlation sequence computed at the symbol rate. It uses only the zeroth cycle since the data are stationary. The summation w.r.t. the lag τ in (32) and the window $W^{(L/2)}(\tau)$ serve the purpose of reducing estimation variance. Our estimator in (24) also exploits the phase shift due to f_e, but invokes cycles different from zero to obtain an estimator tolerant to stationary additive noise (whatever is the noise color or/and the distribution). Furthermore, we have shown that once the frequency offset has been estimated, timing recovery is possible with minimal overhead. This estimate can represent a reasonable initialization for more sophisticated nonlinear timing estimators, such as the one proposed in [5], that require good initial estimates to avoid convergence to local minima.

Finally, in Fig. 10 we compare (27) and (24). The plots were generated with 4-QAM i.i.d. symbols and estimates were averaged over 400 Monte Carlo runs. The other parameters were $P = 8$, $\epsilon = 0.5$, $L = 128$, $L_g = 16$, $N_{zp} = 10^{17}$, and $B_\mu T = 0.05$. In this case the cyclic-correlation-based method exhibited better performance, and additional numerical results (not reported here) have illustrated that the cyclic spectrum outperforms cyclic-correlation-based methods in the data-aided case. With regard to oversampling and noise spectrum shaping, the following remark is of interest.

Remark 3: In all of our simulations we assumed rolloff factor $\alpha = 0.5$, so that $g_c^{(rec)}(t)$ had bandwidth $B_g^{(rec)} < 1.5/T$. As a consequence, the noise samples $v(n)$, obtained by sampling with a rate P/T at the output of $g_c^{(\mathrm{rec})}(t)$, were cor-

[3] In [11] multiplication by $w^*(n)$ is also included (so that $w^*(n)w(n) = \sigma_w^2 = 2$) in order to remove the linear modulation. We can incorporate these terms w.l.o.g. in $x(n)$.

related. Here, we reiterate that the proposed algorithms are m.s.s. consistent independent of the noise color; thus, we do not need to use a receiving filter with bandwidth P/T as in [17], or $P/(2T)$ as in [2], in order to obtain uncorrelated noise samples. Note that increasing the bandwidth of $g_c^{(\mathrm{rec})}(t)$ allows more noise power to pass, thereby reducing the SNR at the sampler.

Remark 4: Comparing Fig. 8(b) with Fig. 9(b), it is clear that the multiplicative effect due to fading (or pattern) noise influences MSE performance more so than the AWGN (note that data (or self) noise is present in both cases). Fading causes a floor effect in the MSE curves [c.f. Figs. 9(b) and 10(b)] reminiscent to that encountered with laser phase noise in optical communications. An algorithm capable of tracking and removing fading effects could remove such an error floor and constitutes an interesting future direction.

D. A Unifying CS Viewpoint

Although cyclostationarity induced by oversampling has been implicitly used in the past to estimate synchronization parameters, the role of cyclic statistics in synchronization has not been studied systematically. Formulating the estimation problem in a more general framework allows not only thorough understanding of existing solutions but also suggests new directions to improve performance when, e.g., colored possibly non-Gaussian additive noise or fading effects are present.

To illustrate this point further, consider the well-known Oerder–Meyr synchronizer [13] (used also in [11]). With our notation, it can be expressed as

$$\hat{\epsilon} = -\frac{1}{2\pi}\ \arg\left\{\sum_{n=0}^{LP-1}|x(n)|^2 e^{-j(2\pi/P)n}\right\} = -\frac{1}{2\pi}\ \arg\{\hat{\mathcal{M}}_{2x}(1;0)\}. \quad (33)$$

The estimator in (33) uses only the zeroth lag (w.r.t. τ) of the cycle-frequency $2\pi/P$ ($k=1$). In contrast, (25) exploits the full information available in the data.

So far we have considered only second-order statistics of $x(n)$, but it is clear that our analysis can be extended to higher (than second)-order cyclic statistics. Joint nondata-aided f_e and ϵ estimators based on the fourth-order cyclic moment, were proposed in [10] for minimum-shift keying (MSK) modulation. In particular the timing estimator reads as follows:

$$\hat{\epsilon} = -\frac{1}{2\pi}\ \arg\left\{\frac{1}{P}\sum_{n=0}^{P-1}|y(n)|e^{-j(2\pi/P)n}\right\} \quad (34)$$

with $n = 0, 1, \cdots, P-1$, and

$$y(n) = \frac{1}{L}\sum_{l=0}^{L-1}[x(n-lP)x^*(n-lP-P)]^2. \quad (35)$$

The presence of $|\cdot|$ in (34) removes f_e. If, on the other hand, $f_e = 0$ or it has been estimated and removed from the data, $|\cdot|$ can be dropped from (34). In this case, inserting (35) into (34), we obtain

$$\hat{\epsilon} = -\frac{1}{2\pi}\ \arg\left\{\frac{1}{LP}\sum_{n=0}^{P-1}\sum_{l=0}^{L-1} \cdot [x(n-lP)x^*(n-lP-P)]^2 e^{-j(2\pi/P)n}\right\}. \quad (36)$$

Making use of the identity in footnote 1, we can express the estimator (34) as

$$\hat{\epsilon} = -\frac{1}{2\pi}\ \arg\left\{\frac{1}{LP}\sum_{n=0}^{LP-1}[x(n)x^*(n-P)]^2 e^{-j(2\pi/P)n}\right\} = -\frac{1}{2\pi}\ \arg\{\hat{\mathcal{M}}_{4x}(1;-P,0,-P)\} \quad (37)$$

where, by definition, $\mathcal{M}_{4x}(k;\tau_1,\tau_2,\tau_3) := (1/P)\ \Sigma_{n=0}^{P-1}E\{x(n)x^*(n+\tau_1)x(n+\tau_2)x^*(n+\tau_3)\}\ \exp(-j2\pi kn/P)$ is the fourth-order cyclic moment of the process $x(n)$; $\mathcal{M}_{4x}$ is periodic with period P and is estimated via

$$\hat{\mathcal{M}}_{4x}(k;\tau_1,\tau_2,\tau_3) = \frac{1}{LP}\sum_{n=0}^{LP-1} x(n)x^*(n+\tau_1) \cdot x(n+\tau_2)x^*(n+\tau_3)e^{-j(2\pi/P)kn}. \quad (38)$$

Under (AS4), $\hat{\mathcal{M}}_{4x}$ in (38) is asymptotically unbiased and m.s.s. consistent [4], and the same property carries over to ϵ in (37). Note that this is true whatever the color and/or the distribution of the additive noise $v(n)$, provided that it is stationary and mixing. This is an interesting property not acknowledged in [10].

Once more, viewing synchronization parameter estimates within the context of CS statistics gives access to a wealth of tools useful to understand statistical properties of estimation algorithms and suggests means of improving them, e.g., we expect that the estimator (37) can be improved by looking at the "global" relationship between the time epoch ϵ and the fourth-order cyclic moment $\mathcal{M}_{4x}(k;\tau_1,\tau_2,\tau_3)$. By exploiting information present in lags different than $\tau_1 = \tau_3 = -P$ and $\tau_2 = 0$, or, by looking at cycles other than $k=1$, we expect noticeable performance gain at the expense of moderate increase in computations.

VII. Conclusions and Discussion

In this paper we proposed methods for estimating frequency offset and symbol timing of a linearly modulated waveform transmitted through a frequency-flat fading channel. The methods relied on the full exploitation of the received signal's cyclostationarity, which is introduced in the data when oversampling the matched filter output. The resulting estimators have desirable features, as they do not require training data and, under mild conditions, they are m.s.s. consistent independent of the color and distribution of the fading distortion or the additive noise. We also illustrated the links with existing estimators relying on cyclostationarity. This unifying interpretation allowed us to establish consistency and suggested means of improving them.

Thorough performance analysis including (even asymptotic) variance expression of $\hat{f}_e$ and $\hat{\epsilon}$ is an interesting research direction along with possible extensions to frequency-selective fading environments. Additional topics include nonlinear least-squares criteria weighted with the inverse covariances of $\hat{\mathcal{M}}_{2x}$ to yield estimators with smallest asymptotic variance among all estimators employing sample cyclic correlations.

ACKNOWLEDGMENT

The first author would like to thank Prof. U. Mengali for introducing him to the synchronization problem, for bringing his attention to [18], and for kindly providing a draft version of [11].

REFERENCES

[1] W. R. Bennett, "Statistics of regenerative digital transmission," *Bell System Tech. J.*, vol. 37, pp. 1501–1542, 1958.
[2] W. C. Dam and D. P. Taylor, "An adaptive maximum-likelihood receiver for correlated Rayleigh-fading channel," *IEEE Trans. Commun.*, vol. 42, pp. 2684–2692, Sept. 1994.
[3] A. V. Dandawate and G. B. Giannakis, "Nonparametric polyspectral estimators for kth-order (almost) cyclostationary processes," *IEEE Trans. Inform. Theory*, vol. 40, pp. 67–84, Jan. 1994.
[4] ———, "Asymptotic theory of mixed time averages and kth-order cyclic-moment and cumulant statistics," *IEEE Trans. Inform. Theory*, vol. 41, pp. 216–232, Jan. 1995.
[5] A. N. D'Andrea, U. Mengali, and M. Morelli, "Symbol timing estimation with CPM modulation," *IEEE Trans. Commun.*, vol. 44, pp. 1362–1371, Oct. 1996.
[6] M. P. Fitz, "Further results in the fast frequency estimation of a single frequency," *IEEE Trans. Commun.*, vol. 42, pp. 862–864, Feb./Mar./Apr. 1994.
[7] H. L. Hurd, "Nonparametric time series analysis of periodically correlated processes," *IEEE Trans. Inform. Theory*, vol. 35, pp. 350–359, Mar. 1989.
[8] R. S. Kennedy, *Fading Dispersive Communication Channels*. New York: Wiley, 1960.
[9] M. Luise and R. Reggiannini, "Carrier recovery in all-digital modems for burst-mode transmissions," *IEEE Trans. Commun.*, vol. 43, pp. 1169–1178, Feb./Mar./Apr. 1995.
[10] R. Mehlan, Y. Chen, and H. Meyr, "A fully digital feedforward MSK demodulator with joint frequency offset and symbol timing estimation for burst mode mobile radio," *IEEE Trans. Veh. Technol.*, vol. 42, pp. 434–443, Nov. 1993.
[11] U. Mengali and M. Morelli, "Data-aided frequency estimation for burst digital transmission," *IEEE Trans. Commun.*, vol. 45, pp. 23–25, Jan. 1997.
[12] R. van Nobelen and D. P. Taylor, "Analysis of the pairwise error probability of interleaved codes on the Rayleigh-fading channel," *IEEE Trans. Commun.*, vol. 44, pp. 456–463, 1996.
[13] M. Oerder and H. Meyr, "Digital filter and square timing recovery," *IEEE Trans. Commun.*, vol. 36, pp. 605–611, May 1988.
[14] A. V. Oppenheim and R. W. Schafer, *Discrete-Time Signal Processing*. Englewood Cliffs, NJ: Prentice-Hall, 1989.
[15] J. G. Proakis, *Digital Communications*, 3rd ed. New York: McGraw Hill, 1995.
[16] T. S. Rappaport, *Wireless Communications: Principles and Practice*. Englewood Cliffs, NJ: Prentice-Hall, 1996.
[17] J. Riba and G. Vazquez, "Bayesian recursive estimation of frequency and timing exploiting the cyclostationarity property," *Signal Process.*, vol. 40, pp. 21–37, Jan. 1994.
[18] K. E. Scott and E. B. Olasz, "Simultaneous clock phase and frequency offset estimation," *IEEE Trans. Commun.*, vol. 43, pp. 2263–2270, July 1995.
[19] M. Tsatsanis, G. B. Giannakis, and G. T. Zhou, "Estimation and equalization of fading channels with random coefficients," *Signal Processing*, vol. 53, pp. 211–229, Sept. 1996.
[20] G. M. Vitetta, D. P. Taylor, and U. Mengali, "Double-filtering receivers for PSK signals transmitted over Rayleigh frequency-flat fading channel," *IEEE Trans. Commun.*, vol. 44, pp. 686–695, June 1996.

Fulvio Gini, (M'93) for photograph and biography, see p. 60 of the January 1998 issue of this TRANSACTIONS.

Georgios B. Giannakis (S'84–M'86–SM'91–F'97) received the Diploma degree in electrical engineering from the National Technical University of Athens, Athens, Greece, in 1981, and the M.Sc. degree in electrical engineering, the M.Sc. degree in mathematics, and the Ph.D. degree in electrical engineering from the University of Southern California, Los Angeles, CA, in 1983, 1986, and 1986, respectively.

After lecturing for a year at USC, he joined the Department of Electrical Engineering, University of Virginia, Charlottesville, where he is currently a Professor. His general interests are in the areas of signal processing, communications, estimation and detection theory, and system identification. His current specific research interests are focused on diversity techniques for channel estimation and multiuser communications, nonstationary and CS signal analysis, wavelets in statistical signal processing, and non-Gaussian signal processing with applications to SAR, array, and image processing.

Dr. Giannakis recieved the IEEE Signal Processing Society's 1992 Paper Award in the area of Statistical Signal and Array Processing (SSAP). He co-organized the 1993 IEEE Signal Processing Workshop on Higher Order Statistics, the 1996 IEEE Workshop on Statistical Signal and Array Processing, and the first IEEE Signal Processing Workshop on Wireless Communications in 1997. He was the co-Guest Editor of two special issues on high-order statistics (*International Journal of Adaptive Control and Signal Processing* and the EURASIP journal *Signal Processing*) and the January 1997 IEEE TRANSACTIONS ON SIGNAL PROCESSING Special Issue on Signal Processing for Advanced Communications. He has served as an Associate Editor for the IEEE TRANSACTIONS ON SIGNAL PROCESSING and the IEEE SIGNAL PROCESSING LETTERS, as Secretary of the Signal Processing Conference Board, and as a Member of the Signal Processing Publications Board and the SSAP Technical Committee. He is a member of the IMS and the European Association for Signal Processing.